



3D bioprinting strategies and their application in studies *in vivo* and *in vitro* animal models for skin regeneration: a concise systematic review and meta-analysis

Rodrigo Souza Mauro¹, Idiberto José Zotarelli-Filho^{1,2*}

¹ FACERES – Faculty of Medicine of Sao Jose do Rio Preto, Sao Paulo, Brazil.

² ABRAN - Associação Brasileira de Nutrologia/Brazilian Association of Nutrology, Catanduva, Sao Paulo, Brazil.

*Corresponding author: Dr. Idiberto José Zotarelli-Filho.

FACERES – Faculty of Medicine of Sao Jose do Rio Preto,
Sao Paulo, Brazil.

Email: dr.idibertzotarelli@faceres.com.br

DOI: <https://doi.org/10.54448/mdnt23206>

Received: 12-20-2022; Revised: 02-26-2023; Accepted: 03-20-2023; Published: 03-25-2023; MedNEXT-id: e23206

Abstract

Introduction: Annually, 50% of medical expenses worldwide stem from damage to the body's tissues and organs. Large skin defects can be caused by tumor excision, venous ulcers, diabetic foot ulcers, and burns. The 3D bioprinting of skin has an advantage compared to other technologies for skin substitutes, the capacity for directional and spatial handling at the cellular level with variable density. **Objective:** It was to identify the most efficient 3D bioprinting strategies and their application in studies *in vivo* and *in vitro* animal models, to demonstrate state of art in skin regeneration, and to direct new clinical research with translational studies.

Methods: The rules of the Systematic Review-PRISMA Platform were followed. The research was carried out from November 2022 to February 2023 and developed based on Scopus, PubMed, Science Direct, Scielo, and Google Scholar. The quality of the studies was based on the GRADE instrument and the risk of bias was analyzed according to the Cochrane instrument. **Results:** A total of 237 articles were found and 97 articles were evaluated in full, and 16 were included and described in the present study. According to the GRADE instrument, most studies (X2 =90.5%>50%) followed a controlled clinical study model and had a good methodological design. the biases did not compromise the scientific basis of the studies. **Conclusion:** Most organotypic skin models have an epidermal layer of keratinocytes and a dermal layer of fibroblasts embedded in an extracellular matrix-based biomaterial. Furthermore, skin comprising epidermis, dermis, and hypodermis stratified with blood vessels, nerves, muscles, and cutaneous appendages

can be fabricated. These findings provided evidence for further advances in translational studies in humans.

Keywords: Skin. Tissue regeneration. Animal models. 3D Bioprinting.

Introduction

As it is in contact with the external environment, the skin is exposed to possible trauma and, despite having a great regenerative capacity, in cases of severe damage, the tissue cell constitution is not fully repaired, which negatively affects the patient's evolution and quality of life. life [1,2]. Annually, 50% of medical expenses worldwide stem from damage to the body's tissues and organs. Large skin defects can be caused by tumor excision, venous ulcers, diabetic foot ulcers, and burns [3,4].

Moreover, basal cell carcinoma (BCC) is the most frequent malignant neoplasm that affects Caucasians, its occurrence worldwide is on the rise. BCC is associated with low mortality and high morbidity and increased costs for the health system. the most adopted therapy is surgical excision, but if the lesion has a very large extension, additional surgery may be necessary to close the wound [4].

Besides, venous ulceration of the lower limbs is a disabling disease of a periodic and chronic character, which affects 1 in every 100 adults throughout life. The usual therapeutic interventions are simple dressings and bandages or compression stockings. However, despite the adoption of these measures, the ulcers can remain open for an indefinite period, requiring the use of skin

grafts to promote healing [5].

A diabetic foot ulcer is a serious problem in the public health system, its worldwide prevalence is 6.3%, affecting mostly patients with type 2 diabetes mellitus; male patients; the elderly, who have low body mass index; hypertensive, and smokers. Furthermore, it is noteworthy that of the amputations performed in patients with diabetes, 85% of these preceded foot ulceration, which evolved with infection and severe gangrene. Skin grafts for tissue reconstruction in patients with the diabetic foot can be used together with the usual treatment [6,7].

In addition, burns are considered very frequent injuries and usually occur in domestic and industrial spaces and situations of confrontation/war. In 2014, the World Health Organization estimated the number of fatal burn victims at 265,000 per year. In addition, a decrease in the overall mortality of burn patients was observed, which was attributed to infection control, intensive care, kidney transplantation, and nutritional support [8,9].

The increase in the functional rehabilitation rate of patients who have suffered this type of trauma is due to progress in learning about burn care and pharmacological knowledge. The treatment of burned patients includes several surgical procedures, among them, primary closure, excision of the burn with skin grafts, and skin analogs. Burn victims mostly survive the injuries, and after hemodynamic stabilization, they must be submitted to wound closure with reconstructive surgeries, to restore the function and aesthetics of the skin. The primary closure of burns consists of closing the lesion after removing dead tissue, it is indicated in small burns, congruent with Langer's skin tension lines to optimize the ideal aesthetic effect. The addition of skin stretching devices to the primary closure also allows its use on larger burns. In the event of a very large wound, additional surgery is required, currently, the combination of excision and autologous graft is the approach of choice for deep dermal burns [9].

Also, the recommended treatment for cutaneous scars is autologous skin transplantation, which can present several complications, such as depigmentation, infections, hypertrophic scars, and obstacles, such as little tissue extension for transplantation. Faced with these difficulties, tissue engineering emerged, offering new possibilities for treatment. The development of research for the creation of skin substitutes for wound closure has progressed rapidly using stem cells and the manipulation of biomaterials [10].

In this sense, 3D bioprinting is defined as the process of technological use of rapid prototypes, thus printing biological components such as cells and their

annexes, thus manufacturing biomedical elements with the greatest possible accuracy to natural tissues. Additive manufacturing creates intrinsically biocompatible 3D arrays by placing biological structures in a substance mediated by computer-aided design (CAD/CAM) technology. It is possible to divide bioprinting technologies into 3 categories through their modeling concept and the material that the print is made from. They are droplet-based bioprinting (DBB), extrusion-based bioprinting (EBB), and photopolymerization-based bioprinting (PBB) [11-13].

In this respect, 3D printing refers to the linear development of thin roofs that conceive a solid 3D structural conformation. It consists of an additive manufacturing technology and can be carried out on a large scale through tissue engineering. The five stages of bioprinting are: scanning the target tissue; fabric model development using cad-cam (computer-aided manufacturing) software; choice of scaffolds and cells of the biomaterial; tissue printing through bioprinter and maturation of the bioprinted tissue. Therefore, 3D bioprinting is a computer-aided (cad) manufacturing technique that places living cells layer by layer of material on scaffolds secured with hydrogel and enables the regulation of individual tissue or organ elements, thus enabling the development of the structure detailed 3d fabric with bioprinting, it is possible to create tailor-made biological tissues with the cad file previously adjusted for printing bioprinting can be performed *in vitro* (when, after cultivation, the 3d constructs are analyzed through *in vitro* viability tests) or *in vivo* (if, after maturation, the tissues are implanted in animals for evaluation). The 3D printing process is divided into tissue pre-bioprinting, bioprinting, and post-bioprinting maturation [14,15].

Still, the 3D bioprinting of skin has an advantage compared to other technologies for skin substitutes, the capacity for directional and spatial handling at the cellular level with variable density. In addition, 3D constructs can be: (1) manipulated into the shape and depth of the lesion and readily printed with high reproducibility through tissue scanning technology; (2) availability of different types of bio-inks (including biological materials with antibiotic properties, growth factors, etc...); (3) tissue can be printed directly onto the surface of the lesion using layer-by-layer deposition; (4) the technique of constructs with pores allows a high cell viability and cell fixation [16].

Added to this, the scientific articles developed about 3D bioprinting as a skin substitute, have gaps in its implementation in humans, highlighting that further research is needed to ensure the safety and feasibility of using this technology in humans [17-20].

Thus, the objective of this study was to identify the most efficient 3D bioprinting strategies and their application in studies *in vivo* and *in vitro* animal models, to demonstrate state of the art in skin regeneration, and to direct new clinical research with studies translational.

Methods

Study Design

The rules of the Systematic Review-PRISMA Platform (Transparent reporting of systematic reviews and meta-analysis (Available in: www.prisma-statement.org/) were followed.

Data sources and research strategy

The search strategies for this systematic review were based on the MeSH Terms: *Skin. Tissue regeneration. Animal models. 3D Bioprinting.* The literary search process was carried out from November 2022 to February 2023 and developed based on Scopus, PubMed, Science Direct, Scielo, and Google Scholar. Also, the combination of the keywords with the booleans "or", "and", and the operator "not" were used to target the scientific articles of interest.

Study Quality and Risk of Bias

The quality of the studies was based on the GRADE instrument, and the risk of bias was analyzed according to the Cochrane instrument. Two independent reviewers (1 and 2) carried out research and study selection. Data extraction was performed by reviewer 1 and fully reviewed by reviewer 2.

Statistical Analysis

A database was built in a Microsoft Excel spreadsheet, which was exported to the Minitab 18® statistical program (version 18. Minitab. LLC. State College. Pennsylvania, USA). The Cohen test was performed to calculate the effect size (Effect Size) and the inverse of the standard error (precision or sample size) was determined to determine the risk of bias in the studies using the Funnel Plot. The Heterogeneity Test (Chi-Square Test – X^2) of the results between the studies was also determined, with $p < 0.05$ with no statistically significant difference, in the 95% CI.

Results and Discussion

Summary of Findings

A total of 237 articles were found. Initially, duplication of articles was excluded. After this process, the abstracts were evaluated and a new exclusion was performed, removing articles that did not include the theme of this article. A total of 97 articles were evaluated in full and 16 were included and described in

the results of the systematic review (**Figure 1**). According to the GRADE instrument, most studies ($X^2 = 90,5\% > 50\%$) followed studies models and had a good methodological design, with $p < 0.05$. Considering the Cochrane tool for risk of bias, the biases did not compromise the scientific basis of the studies.

Figure 1. Study Eligibility (Systematic Review).

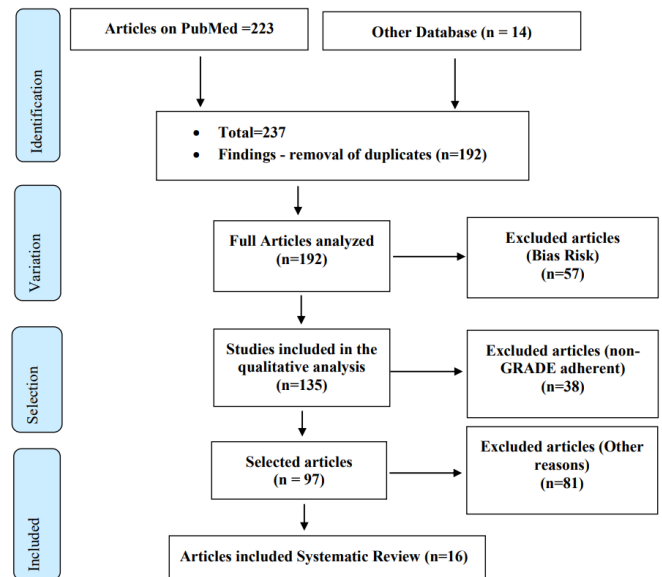
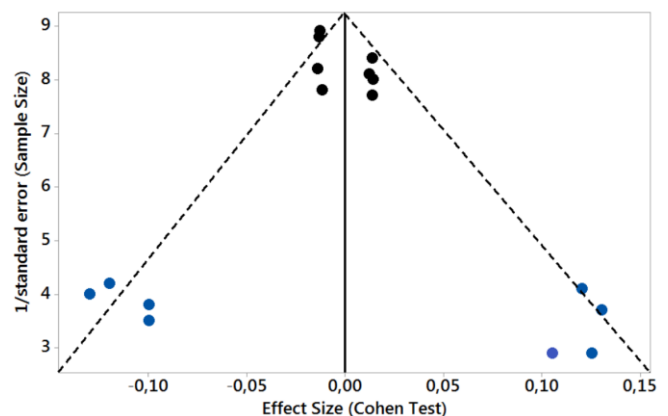


Figure 2 presents the results of the risk of bias of the studies through the Funnel Plot, showing the calculation of the Effect Size (Magnitude of the difference) using the Cohen Test (d). This graph had a symmetrical behavior, not suggesting a significant risk of bias. The blue balls represent studies with a low sample size, showing symmetrical behavior (without risk of bias) according to the Funnel Plot graph in Figure 2.

Figure 2. The symmetrical Funnel Plot (N=16 studies).



Major Findings

Table 1 presents the main studies and their scientific outcomes on the use of 3D printers in skin regeneration, presenting the most efficient 3D bioprinting strategies and their application *in vivo* and *in vitro* clinical studies, as well as directing new clinical research.

Table 1. Major findings about 3D bioprinting in skin regeneration.

Author	Sample Size	Effect Size	Major Outcomes	Follow-Up
Feifei Zhou et al. 2022 [21]	48 rats 3 pigs (4 wounds of 4.5 x 4.5 cm each).	<p>Rat Model: Wound closure time was significantly longer in the FLS group compared to the hydrogel, scaffold, and control groups. H&E staining verified that the wounds in the "FLS" group were reepithelialized on postoperative day 7, while the lesions in the other three groups remained open. Immunostaining of inflammatory cells detected the highest levels of CD3, CD68, and MPO in the control groups, followed by the hydrogel groups and the scaffold groups; while the lowest levels of CD3, CD68, and MPO were observed in the "FLS" treated samples.</p> <p>Pigs model: morphology analysis showed that the closure of the FLS group was significantly higher when compared to the control group, H&E staining showed that sebaceous and follicular glands were only formed in the FLS group.</p> <p>Data were evaluated using two-way ANOVA analysis, showing a 95% confidence interval. $p < 0.05$ considered statistically significant.</p>	<p>The viability of the DLP-based 3D printing strategy combined with biomimetic bio-ink and functional cells for FLS fabrication was observed. The lowest inflammatory response was observed in the group treated with scaffold and FLS. Natural ECM components were selected to design the biomimetic hydrogel bioink to maximally support cell migration and proliferation. <i>In vivo</i> studies have demonstrated that FLS has superior performance in regenerating skin with cutaneous appendages such as follicles in both small and large animals.</p>	<p>Digital photos were taken at intervals of the 4th, 7th, 14th and 21st Postoperative days of the experiment on the dorsal surface of rats. Digital photos were taken 30 days after the experiment on the dorsal surface of pigs.</p>
Nieves Cubo et al. 2016 [22]	4 rats	No control group	<p>The analysis of the <i>in vitro</i> skin proved to be equivalent to skin substitutes and normal human skin, and the expression of keratin K10 was observed. The analysis of the grafted skin in the rats showed a thick, whitish, and wrinkled appearance similar to human skin, histologically it presented characteristics of normal skin, with the expression of keratin K10 and the presence of blood vessels.</p>	8 weeks
Mohammed Albanna et al. 2019 [23]	36 rats 6 pigs	<p>Rat Model: Imprinted skin constructs show significantly reduced time to wound closure when compared to untreated and matrix-treated controls. Imprinted skin closed the wound in 3 weeks compared to 5 weeks for controls. One-way ANOVA analysis. ****$p < 0.0001$, $n = 12$; ***$p < 0.01$, $n = 8$; *$p < 0.05$, $n = 8$. Data presented as mean \pm standard deviation (SD).</p> <p>Pig Model: Open wound size and wound contraction were less in wounds treated with autologous cells compared to other treatments. Wounds treated with autologous cells showed significantly accelerated re-epithelialization compared to all other groups. Wound sizes were analyzed with one-way ANOVA. ***$p < 0.001$, $n = 6$; **$p < 0.01$, $n = 6$; *$p < 0.05$, $n = 6$. Data presented as mean \pm standard deviation (SD).</p>	<p>Analysis of rodent wounds treated with in-situ skin bioprinting showed improved recovery compared to controls with wound closure after 3 weeks compared to 5 weeks for both controls. The printed skin showed high cellularity after 1 week postoperatively with the presence of an organized epidermis aligned with collagen fibers. Analysis of wounds from pigs treated with in-situ bioprinting resulted in an acceleration of 3-week wound closure compared to the other groups.</p>	<p>6 weeks of rodent wound model. 8 weeks of pig wound model.</p>
Leila Roshangar et al. 2021 [24]	12 rats	<p>The analysis resulted in a significant increase in optical density (OD) in the first 48hrs among the 3D bioprinted gel-derived graft compared to the control. Both gel-derived graft 3D bioprinting and gel-derived graft 3D bioprinting with ADSCs significantly increased burn healing and closure. Histological changes in the ADSC group showed neovascularization and denser collagen fibers similar to normal skin.</p> <p>The <i>in vivo</i> analysis of the difference between the natural epithelium, the control group, and the test groups showed no significant change ($p = 0.15$).</p>	<p><i>In vitro</i> analysis showed a significant increase in optical density (OD) in the first 48hrs between 3D bioprinting with gel-derived graft compared to control. Both gel-derived graft 3D bioprinting and gel-derived graft 3D bioprinting with ADSCs significantly increased burn healing and closure. Histological changes in the ADSC group showed neovascularization and denser collagen fibers similar to normal skin. The <i>in vivo</i> analysis of the difference between the natural epithelium, the control group, and the test groups showed no significant change ($p = 0.15$).</p>	21 days

<p>Soojiung Jin et al. 2022 [25]</p>	<p>One male mice</p>	<p>No control group</p>	<p>Constructs were cured using calcium ion and thrombin and incubated for 14 days. It was observed that HFF-1 and HaCaT cells did not mix and remained in layers, with a high proportion of living cells and adequate degree of differentiation. Optimal cell viability conditions were observed when skin constructs were imprinted and cultured using epidermal and dermal cells extracted from rat skin. Data are presented as the mean ± SD of at least three independent experiments. Statistical comparisons between groups were performed using the SPSS program followed by the Studentt-test. A p-value < 0.05 was considered statistically significant.</p>	<p>14 days</p>
<p>Jingge Ma et al. 2021 [26]</p>	<p>Subcutaneous Implantation Model: BALB/naked male mice <i>In Vivo</i> Engraftment Model in Nude Rat Wounds: 9 BALB/Male Nude Rats <i>In Vivo</i> Healing Model of Diabetic Skin Tissue: 10 C57BL/6 male mice</p>	<p>Subcutaneous Implantation Model: Samples obtained from the 2SS-GAM and Co-2SS-GAM groups showed increased positive expression of CD31 compared to the corresponding groups without SS. <i>In Vivo</i> Graft Model in Nude Rat Wounds: A Heart of H&E, showed that closure of the 2SS-GAM, Co-GAM, and Co-2SS-GAM groups showed complete healing with intact dermal structure and complete epithelialization on day 15. <i>In Vivo</i> Healing Model of Diabetic Skin Tissue: Wound beds treated with Co-2SS-GAM scaffolds showed the greatest healing among all groups. Histological examination showed reconstruction of the dermis and epidermis cover and the morphogenesis of the hair follicles at the wound site of the Co-2SS-GAM group on day 15, while insufficient epithelialization was revealed in the other groups.</p>	<p>Subcutaneous Implantation Model: Hematoxylin and eosin (H&E) staining revealed that the number of internal cells in the implants in the groups with loaded cells was much higher than in those without cells. Samples obtained from the 2SS-GAM and Co-2SS-GAM groups showed increased positive CD31 expression compared to the corresponding groups without SS. Several functional human blood vessels were detected in the Co-GAM and Co-2SSGAM samples, while there was no positive reaction in the other groups. Therefore, the instinctive vascularization activity of the 3D bioprinting multicellular scaffolds was confirmed. It should be noted that there were a greater number of human blood vessels in the Co-2SS-GAM samples. <i>In Vivo</i> Graft Model in Nude Rat Wounds: Wound closure at 15 days, the 2SS-GAM, CoGAM, and Co-2SS-GAM groups exhibited the highest rapid wound healing rates. The heart of H&E showed that the closure of the 2SS-GAM, Co-GAM, and Co-2SS-GAM groups showed complete healing with intact dermal structure and complete epithelialization at day 15. The Co-2SS-GAM group had the thinnest epidermis thick among all groups. Inductively coupled plasma optical emission spectroscopy (ICP-OES) showed that wound transplanted with Co-2SS-GAM scaffolds had higher Sr and Si element content than normal murine skin on day 7, while there was no significant difference on completely regenerated skin on day 15. Immunohistochemical staining to assess the degree of vascularity in the dermis showed that the Co-2SS-GAM group exhibited the most increased angiogenesis, followed by the 2SSGAM group, indicating that blood vessel formation in the dermis was significantly promoted by SS during the wound healing process. <i>In Vivo</i> Healing Model of Diabetic Skin Tissue: Wound beds treated with Co-2SS-GAM scaffolds showed the greatest healing among all groups. Histological examination showed reconstruction of the dermis and epidermis cover and the morphogenesis of the hair follicles at the wound site of the Co-2SS-GAM group on day 15, while insufficient epithelialization was revealed in the other groups. In Masson's Trichrome staining and collagen area statistics, the regenerative dermis of the Co-2SS-GAM group exhibited the highest collagen fiber content among the five groups. Statistical analysis: All numerical data were expressed as mean ± standard deviation in the Origin 2017 software (OriginLab, USA) and analyzed by one-way analysis of variance. Significant difference was determined with *p < 0.05, **p < 0.01, ***p < 0.001, ****p < 0.0001.</p>	<p>Subcutaneous Implant Model: 4 weeks <i>In Vivo</i> Graft Model in naked rat wounds: 15 days <i>In Vivo</i> Healing Model of Diabetic Skin Tissue: 15 days</p>
<p>Byoung Soo Kim et al. 2018 [27]</p>	<p>8 BALB/ca-nu/nu mice</p>	<p>Wound closure and revitalization were faster in groups using S-dECM + adipose tissue-derived stem cells (ASC) + endothelial progenitor cells (EPCs)</p>	<p>The <i>in vitro</i> analysis showed that the S-dECM has a tightness and collagen secretion closer to the natural skin that controls it. In the <i>in vivo</i> analysis, wound closure and revitalization were faster in the groups that used S-dECM + adipose tissue-derived stem cells (ASC) + endothelial progenitor cells (EPCs)</p>	<p>21 days</p>

Brian Chang et al. 2020 [28]	10 athymic mice	Cartilage-seeded scaffolds had relatively lower rates of non-surgical site complications compared to nonseeded scaffolds, which had greater surgical site ulceration, although neither was statistically significant.	The analysis of the anatomy and integrity of both groups was maintained. Cartilage-seeded scaffolds had relatively lower rates of nonsurgical site complications compared to nonseeded scaffolds, which had greater surgical site ulceration, although neither was statistically significant. Histology revealed robust soft tissue infiltration and vascularity in both seeded and non-seeded scaffolds and demonstrated impressive maintenance of viable cartilage in seeded scaffolds. Radiology confirmed soft tissue infiltration in all scaffolds and biomechanical modeling suggested stress improvement in scaffolds implanted with cartilage.	24 weeks
Stefanie Michael et al. 2013 [29]	12 BALB/c-nu mice purchased from Charles River and maintained at the local animal care center per institution guidelines	No control group	The imprinted cells formed sheets of multilayered keratinized skin with the ability to secrete collagen. E-cadherin localization patterns are the same as native skin. Cytokeratin 14 was found throughout the epidermis of the printed construct.	12 weeks
Sha Huang et al. 2016 [30]	15 rats	Each experiment was performed independently at least 3 times. Data are expressed as mean \pm SD. Data were analyzed using SPSS for Windows (SPSS Inc., Chicago, IL, USA) and compared using Student's t-test. $P < 0.05$ was considered statistically significant.	<p>3D-ECM induction of sweat gland differentiation <i>in vitro</i>. Epidermal cells differentiate into sweat gland cells, they must lose basic epithelial markers (CK5, CK14) and gain luminal epithelial markers (CK8, CK18). In this regard, a marker conversion can serve as a differentiating indicator in this study.</p> <p>Immunofluorescence staining confirmed the progression of early epidermal differentiation. After 3D-ECM cultivation for 14 days; most cells were positive for CK8 and CK18 in the 3DECM samples incorporating EGF and PD (Eps+PD+EGF group). Both CK8 and CK18 remained co-expressed. However, without EGF, differentiation decreased (Eps+PD group). Stem cells grown in 3D-ECM samples incorporating EGF and DD maintained CK5 and CK14 expression (Eps+DD+EGF group).</p> <p>The mRNA expression of epidermal differentiation markers CK8 and CK18 (group Eps+PD+EGF) was detected ($P < 0.05$). With or without EGF, DD components in 3D-ECM (Eps+DD+EGF group, Eps+DD group) did not promote differentiation of epidermal cells to sweat gland lineages compared to PD components (Eps+PD+EGF group). Thus, the epidermal progenitors in the 3D-ECM samples acquired a favorable environment to mimic their natural fate-determining niche. 3D-ECM regeneration of sweat glands <i>in vivo</i>. 3D-ECM implantation revealed that only mice with 3D-ECM incorporating EGF and PD (Eps+PD+EGF group) showed individual sweat glands (represented by black dots on the paw pads) and the number increased within 10 minutes; however, no obvious black dots were seen in other groups even after 15 minutes. Tissues were stained with DAPI to reveal cellular distribution within the tissue.</p> <p>Fluorescence images of GFP-positive cells were visible more or less in all groups, but efficient epithelial differentiation into sweat glands appeared only in wounds from the groups treated with 3D-ECM incorporating EGF and PD (Eps+PD+EGF group); without any of these factors, only sporadic differentiation occurred. Large numbers of GFP-labeled cells were visible in the stratified epidermis of groups treated with 3D-ECM incorporating EGF and DD (Eps+DD+EGF group). The structure of the preliminarily formed sweat gland presumably reflects that epithelial differentiation depends on the ECM, in addition to perhaps a microenvironment produced by the dermis. For wound healing 14 days after treatment by histology, the tissue-forming ability of 3D-ECM samples was better with EGF and dermis than with other treatments. Notably, sweat glands occurred in newly formed skin with 3D-ECM incorporating EGF and PD (Eps+PD+EGF group). The histology results also indicate the total degradation of the 3D-ECM samples <i>in vivo</i>.</p>	14 days

<p>Lothar Koch et al. 2012 [31]</p>	<p>3D tissue formation experiments were performed with NIH-3T3 mouse albino Swiss fibroblast (DSMZ Braunschweig, Germany) and HaCaT immortalized human keratinocyte cell line (DKFZ, Heidelberg, Germany).</p>	<p>The qualitative analysis of the vitality of the constructs was verified by the Ki67 staining, which showed the fraction of proliferating cells after 10 days of imprinting, the formation of the basal lamina, by the existence of cell junctions were investigated. Adhesive joints ensure tissue cohesion as functioning gap junctions.</p>	<p>The vitality of the 3D cell bilayer structures was verified by the presence of the Ki-67 protein. Immunostaining verified the expression of cadherin located on the membrane 10 days after imprinting. Immunostaining also showed the presence of Cx43 on the membrane 10 days after printing. The scrape loading/dye transfer (SL/DT) test showed the functionality of the skin's gap junctions.</p>
<p>Ferdows Afghah et al. 2020 [32]</p>	<p>Biocompatibility: analyzed after treatment of HDF cells with scaffold extracts. Antibacterial Activity of Block Copolymer Impregnated with Silver Nitrate: Antimicrobial activities of 5 × 5 mm rectangular polymer films were determined by examining the potential for diffusion zone formation using model microorganisms, including Gram-negative <i>P. aeruginosa</i> and <i>E. coli</i>, Gram-positive bacteria <i>S. aureus</i> and yeast <i>C. albicans</i>. Antimicrobial activity was determined by observing the presence of the zone of inhibition around the copolymer films after the incubation period and the diameter of each housing zone was measured and reported in mm.</p>	<p>Biocompatibility: The cytotoxicity of PCL, PCLPPSu, and the corresponding AgNO₃-containing compounds in HDF cells were investigated using the WST-1 colorimetric assay. Exposure of extracts from PCL and PCL-PPSu samples did not affect cell viability in cultured cells compared to control. Antibacterial activity of block copolymer impregnated with silver nitrate: The microorganism density in PCL-PPSu copolymer films was quite high for all microorganisms, While PCLPPSu/AgNO₃ film surfaces no growth was observed for <i>E. coli</i> and <i>P. aeruginosa</i>, in Petri dishes belonging to PCL-PPSu/AgNO₃ film surfaces incubated with <i>E. coli</i> and <i>P. Aeruginosa</i> and the density of <i>C.albicans</i> and <i>S. aureus</i> decreased to their control groups.</p>	<p>The surface hydration and hydrophilicity of the PCL-PPSu group were significantly superior to the control (PCL). The toxicity of PCL, PCLPPSu, and the corresponding AgNO₃containing compounds to HDF cells was evaluated using the WST-1 colorimetric test. The concentration of PCL/AgNO₃ and PCLPPSu/AgNO₃ resulted in a significant loss of cell viability due to the cytotoxic effect of Ag⁺, and the concentration of AgNO₃ was reduced. The incorporation of silver nitrate in the copolymer significantly reduced bacterial adhesion for all investigated microorganisms, the inhibition zone tests demonstrate its effect was more effective against <i>E. coli</i> and <i>C. albicans</i> compared to <i>P. aeruginosa</i> and <i>S. aureus</i>.</p>
<p>Xue Liu et al. 2020 [33]</p>	<p>Vascularized human skin similar to atopic dermatitis: Used IL-4-treated FTS and VFTS constructs to induce key Atopic Dermatitis phenotypes. Inhibition of JAK/STAT results in ADlike skin equivalents: We evaluated the effect of JAK/STAT inhibitors on 3D FTS, VFTS ADlike constructs. JAK inhibitors on vascular formation: analyzed the effect of JAK inhibitors on angiogenesis, using specific anti-CD31 in vascularized dermis.</p>	<p>Full-thickness skin equivalents (FTS) and vascularized full-thickness skin equivalents (VFTS) mimic AD. Histological characterization of normal and atopic dermatitis (AD) type SFT and VFTS. Immunostaining for differentiation markers (loricrin) and cell-cell junction (E-cadherin). In contrast to the FTS and control VFTS, the IL-4exposed AD-type FTS and the DA-type VFTS demonstrate thicker epidermis, intraepidermal edema with clear spaces separating the keratinocytes, and hair loss. terminal differentiation markers (scale bar: 50 μm). (b) Integrity of normal and AD type FTS tight junction barrier function liquid-air interface (ALI) culture from day 6-10 (N=6). TEER values of normal and AD-like VFTS during the ALI culture period from day 6-10 (N=8). (c) Pro-inflammatory cytokine interleukin-1α (IL1α), AD-related chemokine, serum thymus and activation-regulated chemokine (CART) and eotaxin are compared between day 1 and day 10 of ALI under normal and AD-like conditions Fabric FTS and VFTS (N=3).</p>	<p>Bioprinted human skin produced with this protocol for vascularized skin tissue has a layered architecture consisting of dermis and epidermis. Within the expression of KRT 10, filaggrin and loricrin showed adequate stratification and cornification, confirming the complete differentiation of the keratinocytes. High desmoglein expression indicated cadherin junctions between keratinocytes. Integrin β1, laminin 5, and collagen IV were highlighted as indicators of basement membranes for keratinocytes and endothelial cells. Basement membrane protein expressed around endothelial cell lumens demonstrated an integrated characteristic of a stable microvascular network with ECM. 3D reconstructed confocal images provide additional evidence of 3D vascularized dermal structure and epidermal layers, showing the hierarchically ordered polygonal structure of different epidermal layers within a fully differentiated epidermis. For functional validation, we used a high-throughput transepithelial resistance (TEER) measure to assess the barrier function of skin equivalents, demonstrating barrier integrity and values above the limit suggested by OECD guideline 430.</p>

<p>Lobat Tayebi et al. 2018 [34]</p> <p>Viability of membranes seeded with oral fibroblasts and keratinocytes at different culture intervals was evaluated by the prestobue PB assay on days 2, 10 and 20 days)</p>	<p>Statistics were performed using GraphPad Prism 7. The difference was considered significant for a P value < 0.05 by the one-way ANOVA test.</p>	<p>The <i>in vitro</i> test results in this study indicated that the 3D-printed membrane had good biocompatibility as assessed by histology and tissue viability assays. Both human oral fibroblasts and keratinocytes were membrane compatible and proliferated and attached to the material. The epithelial cells formed a continuous epithelium on the membrane surface with no signs of epithelial invasion in the deeper layers of the biomaterial, as confirmed by DAPI staining. This suggested that the 3D-printed membrane was able to achieve the desired barrier function of an <i>in vitro</i> GTR membrane by completely separating the oral epithelial layer from the underlying tissues, allowing the growth and proliferation of other cell types under the tissue layer. connective. These findings indicate the suitability of a 3D-printed hybrid scaffold for potential application in guided tissue regeneration.</p> <p>20 days</p>
<p>Léa J Pourchet et al. 2017 [35]</p> <p>Bioprinted Dermis Characterization: BPS, control (BPD) Differentiation of Dermal Markers: BPS, control (normal human skin)</p>	<p>The printed epidermis expressed all epidermis-related specific markers differentiation and proliferation, such as Ki67, cytokeratin 10, and filaggrin. Immunohistological analysis of bioprinted skin also showed the expression of the number of proteins typically found in the extracellular matrix. Collagen I and V, vimentin, fibrillin, and elastin were abundantly expressed, indicating the complex reconstruction and remodeling of the printed skin.</p>	<p>Mouse NIH 3T3 eGFP fibroblasts showed a homogeneous cell distribution after printing, after 7 days of culture the 3D object was almost completely colonized by cells three-dimensionally. The shear stress values obtained were very low, leading to a negligible impact on cell viability. TCM staining and histological characterization demonstrated that the 3D bioprinted skin was morphologically and biologically equivalent to normal human skin. However, a difference in TCM staining is due to primarily to the fact that bioprinted skins exhibit less extracellular matrix than fully mature human skin. The printed epidermis expressed all specific markers related to epidermal differentiation and proliferation, such as Ki67, cytokeratin 10, and filaggrin. Immunohistological analysis of the bioprinted skin also showed the expression of several proteins typically found in the extracellular matrix. Collagen I and V, vimentin, fibrillin, and elastin were abundantly expressed, indicating the complex reconstruction and remodeling of the skin print. As a final study, an adult-sized ear (8 cm) was printed, using the developed machine and bio-ink, the complex architecture of the object was easily obtained and maintained the 3D organization during culture and the histological and morphological tests were consistent with the previous results.</p> <p>12 days</p>
<p>Su Jeong Lee et al. 2020 [36]</p> <p>The thick swine skin was provided by the Animal and Plant Quarantine Agency, the subcutaneous fat and the epidermis were scratched and removed to isolate the dermal layer. The prepared dermis was thawed and cut for decellularization. The dermis pieces were soaked in 0.25% trypsin in a shaker (300 rpm) for 6 h, and then washed with deionized water three times for 15 minutes each time. The minced tissue was treated with 70% ethanol for 10 h, treated with 3% H₂O₂ for 15 min, and then washed twice for 15 min each time with deionized water. These samples were treated with 1% Triton X-100 in 0.26% EDTA/0.69% Tris for 6 h, followed by the same treatment for an additional 18 h. Samples were washed twice for 15 min each time with deionized water. To manufacture PSP, lyophilized skin tissues were ground to a powder with a cryogenic grinder Freezer/Mill, Spex Sampleprep, Rickmansworth, (UK) and filtered through a 100 µm pore mesh.</p>	<p>Qualitative Analysis of Printed Skin: DAPI and H&E staining confirmed the state of decellularization of PSP, cell nuclei in decellularized skin were not stained in comparison to those of normal skin cells, while tissue ECM was maintained. Metabolic Activity and Viability of Cells Printed on PSP Inks: Cell viability analysis resulted in the proportion of live cells being 75% in the cell-loaded construct. The metabolic activity of the printed cells steadily increased during the 7 days in all samples, in particular, the cells printed with the 10 mg/mL PSP ink formulation showed the highest metabolic activity compared to the cells printed with other bio-inks. In the 20 mg/mL PSP ink, cellular activity was even lower than in the 10 mg/mL PSP ink samples or the 2% alginate control ink sample; indicating that a high concentration of extracellular matrix inhibits cell growth. Quantitative Analysis of Extracellular Matrix Components: As shown, the viscosity measured at increasing concentrations of PSP from 10–20 mg/mL was significantly increased compared to just 2% alginate, indicating that PSP inks allow the fabrication of 3D printed constructs with adequate viscosity properties.</p>	<p>In this study, a minimum concentration of 2% alginate was selected and the viscosity was compared by mixing PSP at two concentrations. As shown, the viscosity measured at increasing concentrations of PSP from 10–20 mg/mL was significantly increased compared to just 2% alginate, indicating that PSP inks allow the fabrication of 3D printed constructs with adequate viscosity properties. Cell viability analysis resulted in the proportion of live cells being 75% in the cell-loaded construct. The metabolic activity of the printed cells steadily increased during the 7 days in all samples, in particular, the cells printed with the 10 mg/mL PSP ink formulation showed the highest metabolic activity compared to the cells printed with other bio-inks. In the 20 mg/mL PSP ink, cellular activity was even lower than in the 10 mg/mL PSP ink samples or the 2% alginate control ink sample; indicating that a high concentration of extracellular matrix inhibits cell growth. 3D printed cell constructs were grown using PSP ink, and quantitation analysis showed that the proportion of elastin that was well retained, particularly the PSP was significantly increased when compared to the 2% alginate control ink sample. Results are similar to cellular metabolic activity analysis (WST-1 and live/dead staining). The results suggested the potential as a 3D printing material of PSP inks, evaluating cellular metabolic activity as well as collagen production in cell-loaded 3D constructs using 10 mg/mL of PSP ink.</p> <p>7 days</p>

According to the findings of the present study, three-dimensional (3D) skin organotypic models have received enormous attention for *in vivo* animal models and two-dimensional *in vitro* assays. Most organotypic skin models have an epidermal layer of keratinocytes and a dermal layer of fibroblasts embedded in an extracellular matrix (ECM)-based biomaterial. ECM provides mechanical support and biochemical signals to cells. Advances and future possibilities in modifying ECM-based biomaterials to recreate disease-like skin models are highlighted given the importance of organotypic skin models in disease modeling [20].

In this regard, three-dimensional (3D) bioprinted skin equivalents are highlighted as the new gold standard for alternative models to animal testing, as well as for full-thickness wound healing. 3D bioprinting methods and notable features of recent studies are classified as advances in materials, structures, and functions. In this regard, one can fabricate skin comprising the epidermis, dermis, and hypodermis stratified with blood vessels, nerves, muscles, and skin appendages [16].

In this context, the systems used for bioprinting may include methods: inkjet, microextrusion, laser, and stereolithography. The inkjet method is based on the accommodation of droplets organized at the cellular level through weight, heat, or acoustics with high performance. The disadvantages of this method include limiting the viscosity of the bio-ink (requiring greater ejection force for greater viscosities), depending on the mechanism of the printers, the fabric can also be exposed to temperature and high frequency [1,2].

The microextrusion method makes use of mechanical or pneumatic extrusion of spheres of materials composed of cells mixed with hydrogels, the compound is chemically or physically solidified to form the 3D construct. Microextrusion enables a wide variety of biomaterials, including materials with high viscosity and density, but in general, they have lower cell viability than the inkjet printer method [2-4].

Also, the laser printing method uses a laser beam directed at a layer of biological material that is propelled with high pressure to a surface, this method is not limited by cell density but has the disadvantage of a decreased flow rate and the Possibility of residues in the final product that acts as a laser-driven transfer substrate [5].

Still, the stereolithography method employs photopolymer bioprinting through light control to solidify and generate a construct, its benefits are high precision and speed, and it can be applied in scaffolds (high-precision fabrics with porous structures), to increase vitality cells, but this method needs a transparent biological material to allow the passage of light [1,6].

Conclusion

Most organotypic skin models have an epidermal layer of keratinocytes and a dermal layer of fibroblasts embedded in an extracellular matrix-based biomaterial. Furthermore, skin comprising epidermis, dermis, and hypodermis stratified with blood vessels, nerves, muscles, and cutaneous appendages can be fabricated. These findings provided evidence for further advances in translational studies in humans.

Acknowledgement

Not applicable.

Ethical Approval

Not applicable.

Informed consent

Not applicable.

Funding

Not applicable.

Data sharing statement

No additional data are available.

Conflict of interest

The authors declare no conflict of interest.

Similarity check

It was applied by Ithenticate®.

About the License

© The authors (s) 2023. The text of this article is open access and licensed under a Creative Commons Attribution 4.0 International License.

References

1. Roediger B, Schlapbach C. T cells in the skin: Lymphoma and inflammatory skin disease. *J Allergy Clin Immunol.* 2022 Apr;149(4):1172-1184. doi: 10.1016/j.jaci.2022.02.015.
2. Hu W, Shang R, Yang J, Chen C, Liu Z, Liang G, He W, Luo G. Skin $\gamma\delta$ T Cells and Their Function in Wound Healing. *Front Immunol.* 2022 Apr 11;13:875076. doi: 10.3389/fimmu.2022.875076.
3. Bay L, Ring HC. Human skin microbiota in health and disease: The cutaneous communities' interplay in equilibrium and dysbiosis: The cutaneous communities' interplay in equilibrium and dysbiosis. *APMIS.* 2022 Dec;130(12):706-

718. doi: 10.1111/apm.13201.
4. Băicoianu-Nițescu LC, Gheorghe AM, Carsote M, Dumitrascu MC, Sandru F. Approach of Multiple Endocrine Neoplasia Type 1 (MEN1) Syndrome-Related Skin Tumors. *Diagnostics (Basel)*. 2022 Nov 12;12(11):2768. doi: 10.3390/diagnostics12112768.
 5. Song MSH, Baldwin AJ, Wormald JCR, Coleman C, Chan JKK. Outcomes of Free Flap Reconstruction for Chronic Venous Ulceration in the Lower Limb: A Systematic Review. *Ann Plast Surg*. 2022 Sep 1;89(3):331-335. doi: 10.1097/SAP.0000000000003249. Epub 2022 Jun 11. PMID: 35703233.
 6. Ziegler D, Tesfaye S, Spallone V, Gurieva I, Al Kaabi J, Mankovsky B, Martinka E, Radulian G, Nguyen KT, Stirban AO, Tankova T, Varkonyi T, Freeman R, Kempler P, Boulton AJ. Screening, diagnosis and management of diabetic sensorimotor polyneuropathy in clinical practice: International expert consensus recommendations. *Diabetes Res Clin Pract*. 2022 Apr;186:109063. doi: 10.1016/j.diabres.2021.109063. Epub 2021 Sep 20. PMID: 34547367.
 7. Dayya D, O'Neill OJ, Huedo-Medina TB, Habib N, Moore J, Iyer K. Debridement of Diabetic Foot Ulcers. *Adv Wound Care (New Rochelle)*. 2022 Dec;11(12):666-686. doi: 10.1089/wound.2021.0016.
 8. Palackic A, Duggan RP, Campbell MS, Walters E, Branski LK, Ayadi AE, Wolf SE. The Role of Skin Substitutes in Acute Burn and Reconstructive Burn Surgery: An Updated Comprehensive Review. *Semin Plast Surg*. 2022 Apr 12;36(1):33-42. doi: 10.1055/s-0042-1743455.
 9. Hebron C, Mehta K, Stewart B, Price P, Potokar T. Implementation of the World Health Organization Global Burn Registry: Lessons Learned. *Ann Glob Health*. 2022 May 18;88(1):34. doi: 10.5334/aogh.3669.
 10. Talbott HE, Mascharak S, Griffin M, Wan DC, Longaker MT. Wound healing, fibroblast heterogeneity, and fibrosis. *Cell Stem Cell*. 2022 Aug 4;29(8):1161-1180. doi: 10.1016/j.stem.2022.07.006.
 11. Panja N, Maji S, Choudhuri S, Ali KA, Hossain CM. 3D Bioprinting of Human Hollow Organs. *AAPS PharmSciTech*. 2022 May 10;23(5):139. doi: 10.1208/s12249-022-02279-9.
 12. Shukla P, Yeleswarapu S, Heinrich MA, Prakash J, Pati F. Mimicking tumor microenvironment by 3D bioprinting: 3D cancer modeling. *Biofabrication*. 2022 May 31;14(3). doi: 10.1088/1758-5090/ac6d11.
 13. Pasierb A, Jezierska M, Karpuk A, Czuwara J, Rudnicka L. 3D skin bioprinting: future potential for skin regeneration. *Postepy Dermatol Alergol*. 2022 Oct;39(5):845-851. doi: 10.5114/ada.2021.109692.
 14. Montesdeoca CYC, Stocco TD, Marciano FR, Webster TJ, Lobo AO. 3D Bioprinting of Smart Oxygen-Releasing Cartilage Scaffolds. *J Funct Biomater*. 2022 Nov 17;13(4):252. doi: 10.3390/jfb13040252.
 15. Gupta S, Bit A. 3D bioprinting in tissue engineering and regenerative medicine. *Cell Tissue Bank*. 2022 Jun;23(2):199-212. doi: 10.1007/s10561-021-09936-6.
 16. Kang MS, Jang J, Jo HJ, Kim WH, Kim B, Chun HJ, Lim D, Han DW. Advances and Innovations of 3D Bioprinting Skin. *Biomolecules*. 2022 Dec 27;13(1):55. doi: 10.3390/biom13010055.
 17. Zhang M, Zhang C, Li Z, Fu X, Huang S. Advances in 3D skin bioprinting for wound healing and disease modeling. *Regen Biomater*. 2022 Dec 19;10:rbac105. doi: 10.1093/rb/rbac105.
 18. Li M, Sun L, Liu Z, Shen Z, Cao Y, Han L, Sang S, Wang J. 3D bioprinting of heterogeneous tissue-engineered skin containing human dermal fibroblasts and keratinocytes. *Biomater Sci*. 2023 Feb 10. doi: 10.1039/d2bm02092k.
 19. Aliberti F, Paolin E, Benedetti L, Cusella G, Ceccarelli G. 3D bioprinting and Rigenera® micrografting technology: A possible countermeasure for wound healing in spaceflight. *Front Bioeng Biotechnol*. 2022 Aug 30;10:937709. doi: 10.3389/fbioe.2022.937709.
 20. Phang SJ, Basak S, Teh HX, Packirisamy G, Fauzi MB, Kuppasamy UR, Neo YP, Looi ML. Advancements in Extracellular Matrix-Based Biomaterials and Biofabrication of 3D Organotypic Skin Models. *ACS Biomater Sci Eng*. 2022 Aug 8;8(8):3220-3241. doi: 10.1021/acsbomaterials.2c00342.
 21. Zhou F, Hong Y, Liang R, Zhang X, Liao Y, Jiang D, Zhang J, Sheng Z, Xie C, Peng Z, Zhuang X, Bunpetch V, Zou Y, Huang W, Zhang Q, Alakpa EV, Zhang S, Ouyang H. Rapid printing of bio-inspired 3D tissue constructs for skin regeneration. *Biomaterials*. 2020 Nov;258:120287. doi: 10.1016/j.biomaterials.2020.120287.
 22. Cubo N, Garcia M, Del Cañizo JF, Velasco D, Jorcano JL. 3D bioprinting of functional human skin: production and in vivo analysis. *Biofabrication*. 2016 Dec 5;9(1):015006. doi: 10.1088/1758-5090/9/1/015006.

23. Albanna M, Binder KW, Murphy SV, Kim J, Qasem SA, Zhao W, Tan J, El-Amin IB, Dice DD, Marco J, Green J, Xu T, Skardal A, Holmes JH, Jackson JD, Atala A, Yoo JJ. In Situ Bioprinting of Autologous Skin Cells Accelerates Wound Healing of Extensive Excisional Full-Thickness Wounds. *Sci Rep.* 2019 Feb 12;9(1):1856. doi: 10.1038/s41598-018-38366-w.
24. Roshangar L, Rad JS, Kheirjou R, Khosroshahi AF. Using 3D-bioprinting scaffold loaded with adipose-derived stem cells to burns wound healing. *J Tissue Eng Regen Med.* 2021 Jun;15(6):546-555. doi: 10.1002/term.3194.
25. Jin S, Oh YN, Son YR, Kwon B, Park JH, Gang MJ, Kim BW, Kwon HJ. ThreeDimensional Skin Tissue Printing with Human Skin Cell Lines and Mouse SkinDerived Epidermal and Dermal Cells. *J Microbiol Biotechnol.* 2022 Feb 28;32(2):238-247. doi: 10.4014/jmb.2111.11042.
26. Ma J, Qin C, Wu J, Zhang H, Zhuang H, Zhang M, Zhang Z, Ma L, Wang X, Ma B, Chang J, Wu C. 3D Printing of Strontium Silicate Microcylinder-Containing Multicellular Biomaterial Inks for Vascularized Skin Regeneration. *Adv Healthc Mater.* 2021 Aug;10(16):e2100523. doi: 10.1002/adhm.202100523.
27. Kim BS, Kwon YW, Kong JS, Park GT, Gao G, Han W, Kim MB, Lee H, Kim JH, Cho DW. 3D cell printing of in vitro stabilized skin model and in vivo pre-vascularized skin patch using tissue-specific extracellular matrix bioink: A step towards advanced skin tissue engineering. *Biomaterials.* 2018 Jun;168:38-53. doi: 10.1016/j.biomaterials.2018.03.040.
28. Chang B, Cornett A, Nourmohammadi Z, Law J, Weld B, Crotts SJ, Hollister SJ, Lombaert IMA, Zopf DA. Hybrid Three-Dimensional-Printed Ear Tissue Scaffold With Autologous Cartilage Mitigates Soft Tissue Complications. *Laryngoscope.* 2021 May;131(5):1008-1015. doi: 10.1002/lary.29114.
29. Michael S, Sorg H, Peck CT, Koch L, Deiwick A, Chichkov B, Vogt PM, Reimers K. Tissue engineered skin substitutes created by laser-assisted bioprinting form skin-like structures in the dorsal skin fold chamber in mice. *PLoS One.* 2013;8(3):e57741. doi: 10.1371/journal.pone.0057741.
30. Huang S, Yao B, Xie J, Fu X. 3D bioprinted extracellular matrix mimics facilitate directed differentiation of epithelial progenitors for sweat gland regeneration. *Acta Biomater.* 2016 Mar 1;32:170-177. doi: 10.1016/j.actbio.2015.12.039.
31. Koch L, Deiwick A, Schlie S, Michael S, Gruene M, Coger V, Zychlinski D, Schambach A, Reimers K, Vogt PM, Chichkov B. Skin tissue generation by laser cell printing. *Biotechnol Bioeng.* 2012 Jul;109(7):1855-63. doi: 10.1002/bit.24455.
32. Afghah F, Ullah M, Seyyed Monfared Zanjani J, Akkus Sut P, Sen O, Emanet M, Saner Okan B, Culha M, Menceloglu Y, Yildiz M, Koc B. 3D printing of silver-doped polycaprolactone-poly(propylene succinate) composite scaffolds for skin tissue engineering. *Biomed Mater.* 2020 Apr 15;15(3):035015. doi: 10.1088/1748-605X/ab7417.
33. Liu X, Michael S, Bharti K, Ferrer M, Song MJ. A biofabricated vascularized skin model of atopic dermatitis for preclinical studies. *Biofabrication.* 2020 Apr 9;12(3):035002. doi: 10.1088/1758-5090/ab76a1.
34. Tayebi L, Rasoulianboroujeni M, Moharamzadeh K, Almela TKD, Cui Z, Ye H. 3Dprinted membrane for guided tissue regeneration. *Mater Sci Eng C Mater Biol Appl.* 2018 Mar 1;84:148-158. doi: 10.1016/j.msec.2017.11.027.
35. Pourchet LJ, Thepot A, Albouy M, Courtial EJ, Boher A, Blum LJ, Marquette CA. Human Skin 3D Bioprinting Using Scaffold-Free Approach. *Adv Healthc Mater.* 2017 Feb;6(4). doi: 10.1002/adhm.201601101.
36. Lee SJ, Lee JH, Park J, Kim WD, Park SA. Fabrication of 3D Printing Scaffold with Porcine Skin Decellularized Bio-Ink for Soft Tissue Engineering. *Materials (Basel).* 2020 Aug 10;13(16):3522. doi: 10.3390/ma13163522.

